RSC Advances

This is an *Accepted Manuscript*, which has been through the Royal Society of Chemistry peer review process and has been accepted for publication.

Accepted Manuscripts are published online shortly after acceptance, before technical editing, formatting and proof reading. Using this free service, authors can make their results available to the community, in citable form, before we publish the edited article. This *Accepted Manuscript* will be replaced by the edited, formatted and paginated article as soon as this is available.

You can find more information about *Accepted Manuscripts* in the Information for Authors.

Please note that technical editing may introduce minor changes to the text and/or graphics, which may alter content. The journal's standard Terms & Conditions and the Ethical guidelines still apply. In no event shall the Royal Society of Chemistry be held responsible for any errors or omissions in this *Accepted Manuscript* or any consequences arising from the use of any information it contains.

ROYAL SOCIETY OF CHEMISTRY

www.rsc.org/advances

The effect of artificial grain boundaries on magneto-transport properties of charge ordered-ferromagnetic nanocomposites

Kalipada Das*, B. Satpati and I. Das

Saha Institute of Nuclear Physics, 1/AF, Bidhannagar, Kolkata-700064, India

E-mail: kalipada.das@saha.ac.in

Abstract

Nanocomposites of charge ordered insulating $Pr_{0.67}Ca_{0.33}MnO_3$ (PCMO) and ferromagnetic metallic $La_{0.67}Sr_{0.33}MnO_3$ (LSMO) nanoparticles have been prepared by chemical synthesis. Transport and magneto-transport properties of nanocrystalline LSMO and the PCMO - LSMO nanocomposites have been studied in detail. At low temperature region upturn of resistivity for both the compounds were observed. The upturn of resistivity is strongly influenced by the external magnetic field. The results are analyzed considering intergranular spin polarized tunneling model. Our study reveals spin polarized tunneling (SPT) is the dominant mechanism leading to the rise in resistivity with lowering the temperature at low temperature region. It also indicates that SPT through the grain boundary is significantly modified in nanocomposite compounds which leads to the enhancement of magnetoresistance and low field magnetoconductance compared to LSMO nanoparticles.

1. Introduction

During last two decades an enormous attention has been paid to study the physical properties of doped perovskite manganite [1-10]. Due to the presence of a lot of intriguing phenomena such as colossal magnetoresistance effect, metal insulator transition, charge ordering and magnetic field induced metamagnetic transition *etc.* in doped manganites; This field becomes an intense field of current research. Except the polycrystalline bulk compounds another field of growing interest of doped manganites is observation of fascinating behavior in their lower dimension. It is well documented that the physical properties of doped manganites are greatly modifies in their nanostructure forms [3-6]. Effects of internal stress by variation of trivalent ion radius or particle size reduction, grain boundaries, grain size and crystallinity on magnetoresistance of doped manganites had been extensively studied [11-15]. Many attempts have been made to explain the electrical transport and magnetotransport behavior of those compounds. By assuming that the electrical transport in a material is dominated

RSC Advances Accepted Manuscript

by evolution with temperature and external magnetic field of two different kinds of parallel connected channel Andres *et al.* proposed a macroscopic model [16]. In their model the electronic transport and magnetoresistance are determined by the relative weight of the channels. Other model proposed by Wagner *et al.* where negative MR is scaled with Brillouin function in ferromagnetic region [17]. To describe the electronic transport especially at the low temperature region Hwang *et al.* proposed the spin polarized tunneling model in polycrystalline compound through the grain boundaries [18]. This model is now widely used to understand the adequate elucidation of electronic transport and influence of magnetic field in it for polycrystalline compounds at low temperature [19-22].

Generally for granular system the effect of grain boundaries and width of the barrier on electronic and magnetotransport properties are significant [23, 24]. Sharp drop of magnetoresistance at very low field region correspond the spin dependent effect due to different magnetization orientation of neighboring grains. Whereas at high magnetic field regime, almost linear behavior is commonly observed, this is connected with the magnetic behavior of the grain boundary that can be different from the bulk material [25].

In our present study we report magnetic, electronic and magneto-transport behavior of the LSMO nanoparticles and PCMO - LSMO nanocomposites in detail. Low temperature upturn in resistivity for both compounds are attempted to describe using various model. Enhancement of magnetoresistance and low field magnetoconductance in nanocomposites are analyzed taking into account spin polarized tunneling (SPT) through grain boundary at lower temperature.

2. Experimental Section

2.1. Sample preparation, characterization and measurements

Nanocrystalline LSMO and nanocomposites have been prepared by well known sol-gel route. For preparation of nanocrystalline LSMO the starting elements were pre-heated La_2O_3, $Sr(NO_3)_2$ and MnO_2 with the purity of greater than 99.99%. The appropriate amount of oxides have been converted to their nitrates form by using nitric acid. Suitable amount of citric acid was added with the clear water solution of the nitrates. Subsequently mixture was slowly evaporated at 80-90^0 C by using the water bath until the gel was formed. By decomposing the gel black porous powder was formed. After pelletizing the black powder it was heat treated for 4 hours at 950^0 C to get nanocrystalline LSMO.

For preparation of the nanocomposites, first we prepared PCMO nanoparticles by above mentioned route using preheated Pr_6O_{11}, $CaCO_3$ and MnO_2. Crystalline nanostructure was formed by heat treatment of decomposed gel at 950^0 C for 4 hours. Suitable amount of the LSMO gel (depending upon the required thickness (in present study it is ~ 10 nm)) was prepared by the same route and the prepared PCMO nanoparticles were mixed in the LSMO gel at the last stage of the gel formation and stirred conteneously. Finaly one part of the pelletized black pourous powder was heat treaed at 900^{0}C for 4 hours (Nanocomposite-1) and another part at 850^{0}C for 4 hours (Nanocomposite-2).

Room temperature x-ray diffraction study was carried out for four prepared samples (LSMO, PCMO, Nanocomposite-1 and Nanocomposite-2) by using Rigaku diffractometer in Brag-Brentano geometry using Cu-Kα source having wavelength 1.54 Å. The Transmission electron microscopy (TEM) measurements were carried out using FEI, Tecnai G^2 F30, S-Twin microscope operating at 300 kV. The microscope was equipped with a high-

RSC Advances Accepted Manuscript

angle annular dark field detector from Fischione (model 3000) and a scanning unit. The compositional analysis was performed using energy dispersive X-ray spectroscopy (EDS, EDAX Inc.) and energy-filtered TEM (EFTEM) measurements using Gatan imaging filter, Quantum SE (model 963) attachment in the same microscope. The sample was dispersed in isopropanol using ultrasonic bath, mounted on a carbon coated Cu grid, dried, and used for TEM measurements.

Electronic transport and magneto-transport properties of LSMO nanoparticles and nanocomposite compound have been performed by usual four probe method. Magnetization as a function of magnetic field measurements is carried out using superconducting quantum interference device (SQUID) (Quantum Design).

3. Experimental Results and Discussion

X-ray diffraction measurements at the room temperature indicate the single phase nature of the LSMO and PCMO nanoparticles. In case of the nanocomposites no additional phase was found except their parent compounds (shown in Fig. 1). The grain size of the LSMO and PCMO were estimated from the x-ray line width broadening (excluding the instrumental broadening) and it was found to be ~28 nm and ~46 nm for LSMO and PCMO respectively. The lattice parameters of the nanostructure compounds were estimated by utilizing Rietveld refinement technique (using FULLPROF program). According to the earlier reports on the structural properties of doped manganites bulk LSMO and PCMO possesses $R\bar{3}c$ and *Pnma* space group symmetry respectively [26]. In the present case, the x-ray diffraction pattern of LSMO and PCMO nanoparticles was indexed considering the $R\bar{3}c$ and *Pnma* space groups respectively. The obtained latticeparameters of the parrent compounds (LSMO and PCMO) were summarized in Table-1. However for nanocomposites, since the space groups of the parrent compounds are very close to each other, it is difficult to distinguish the two phases from x-ray diffraction patterns.

RSC Advances Accepted Manuscript

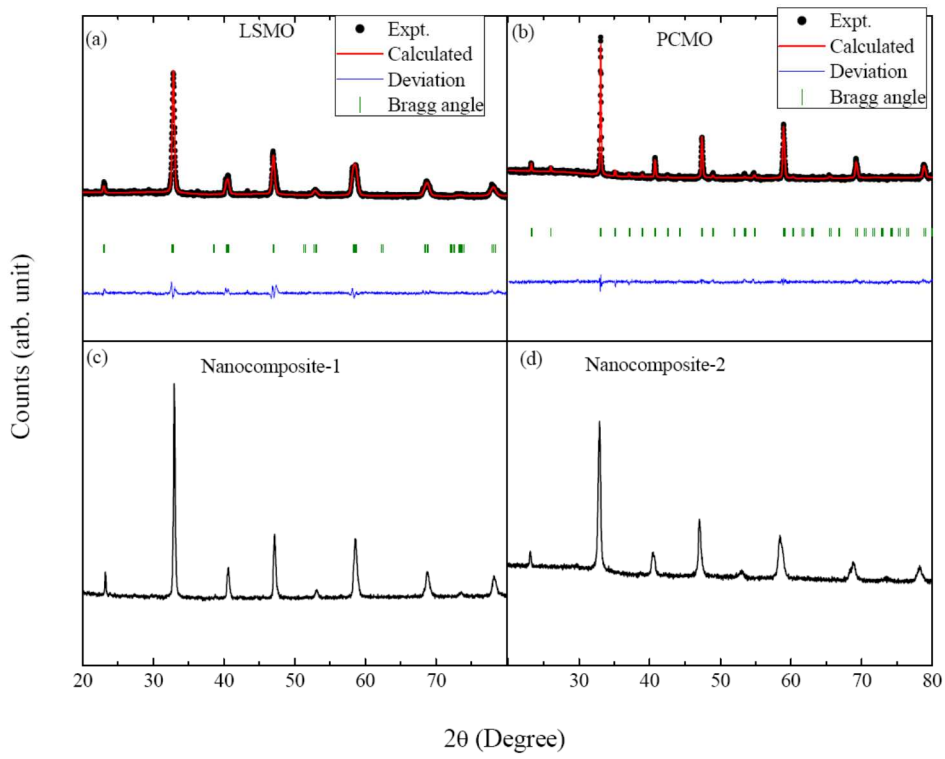

Figure 1. Plot of the Rietveld refinement of x-ray diffraction data of the (a) LSMO and (b) PCMO nanoparticles. (c) and (d) represent the x-ray diffraction patterns of the Nanocomposite-1 and Nanocomposite-2 respectively.

Table 1. Refined structural parameters of the nanostructure compounds.

Compound	Space group	Lattice parameters (Å)
LSMO	$R\bar{3}c$	a = 5.482 b = 5.482 c = 13.359
PCMO	*Pnma*	a = 5.434 b = 7.679 c = 5.431

The nanostructures compounds were further characterized by TEM measurements. In our present report one representative high resolution TEM (HRTEM) image from Nanocomposite-1 sample is shown in Fig. 2. In order to understand the nanocomposite nature of this structure, we have analyzed HRTEM data carefully. Here we have measured lattice spacing from different regions as marked by red and blue boxes and corresponding Fourier filtered images are shown by numbered boxes. The measured lattice spacing from all the red regions are 2.75 Å and from the blue region is 3.81 Å. The interplaner spacing of orthorhombic LSMO (112) is 2.75Å (JCPDS card # 53-0057) and that of orthorhombic PCMO (101) is 3.81Å (JCPDS card # 89-0795). So the measured lattice spacing from

RSC Advances Accepted Manuscript

different regions indicate the formation of nanocomposite structure. However one should note that this lattice spacing of LSMO may match with some other spacing of PCMO with different crystal symmetry.

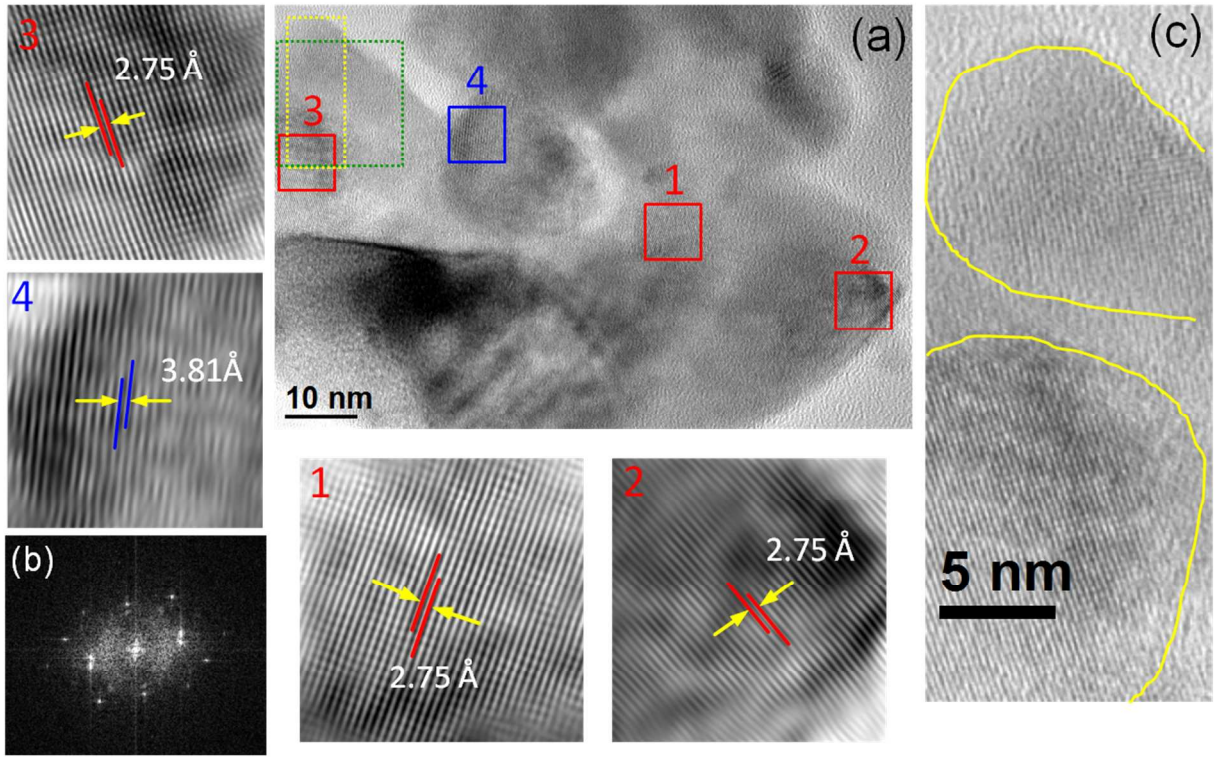

Figure 2. (a) HRTEM image of nanocomposite structure showing lattice fringes, magnified images from different boxed area is shown on both sides indicated by arrows, (b) and (c) represents the FFT pattern and magnified image from a region marked by the green and yellow dotted box in (a), respectively, showing two crystal grains oriented differently and separated by an amorphous region.

Fig. 2(a) further showing that the complete structure is an interconnected grains. The fast Fourier transform (FFT) image in Fig. 2(b) from a region marked by dotted green box and a magnified image in Fig. 2(c) from a yellow dotted box where one can see two crystal grains are oriented by a small angle and amorphous layer in between. We have investigated such several regions of LSMO (shell) regions and observed that in most cases crystals grains are separated by such amorphous layers. Amorphous layer was confirmed by tilting the specimen in different zone axes.

RSC Advances Accepted Manuscript

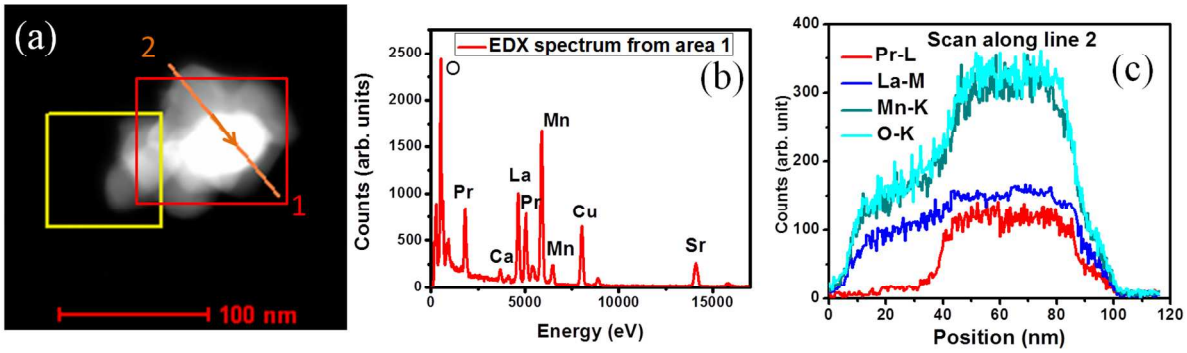

Figure 3. (a) STEM-HAADF image, (b) EDX spectrum from a region marked by area 1 in (a). (c) Drift corrected (yellow box) EDX line scan along line 2 in (a).

We have done the analysis of the effect of enhanced grain boundaries in case of nanocomposites on transport and magneto-transport properties in the later part of this article. To investigate the chemical composition of the nanocomposite structures, we have performed high-angle annular dark field (HAADF) analysis. Fig. 3(a) shows the STEM-HAADF image and this Z-contrast image also showing nanocomposite nature but possibility of different grain thickness (and hence brighter contrast due to higher thickness) cannot be ruled out here. Fig. 3(b) is the corresponding EDX spectrum from area 1 indicating the presence of all the constituent elements of the PCMO-LSMO nanocomposite structure. The Cu signal is due to the Cu-grid. To comfirm further nanocomposite nature we have done line scan analysis which clearly showing that the brighter region in Fig. 3(a) is Pr enriched.

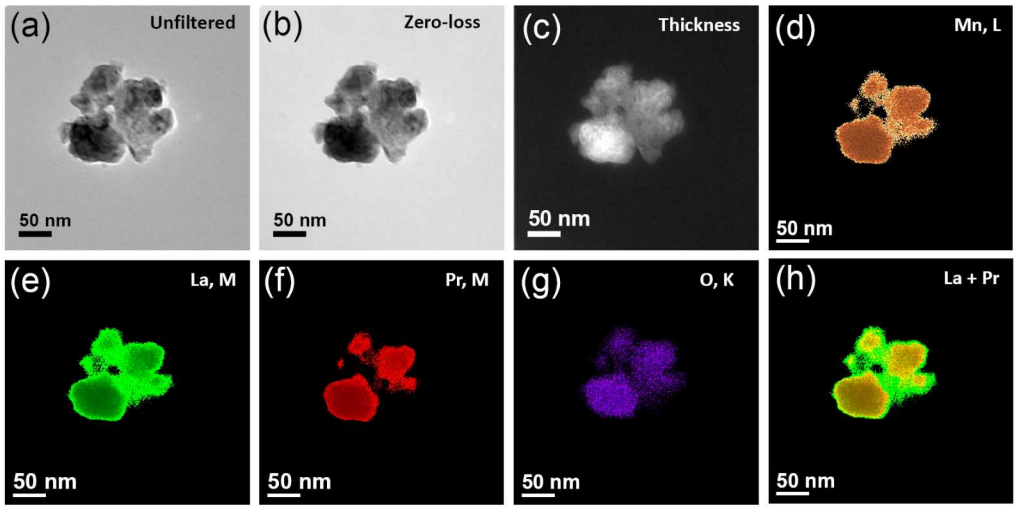

Figure 4. (a-h) EFTEM images taken from a nanocomposite structure, (a) unfiltered image, (b) zero-loss image, (c) relative thickness map, (d) chemical map of Mn, (e) chemical map of La, (f) chemical map of Pr, (g) chemical map of O, (h) composite image showing La (green) and Pr (red), indicating the locations of two different atoms across the PCMO-LSMO nanocomposite structures.

RSC Advances Accepted Manuscript

To identify further the nanocomposite nature of these structures we have carried out chemical imaging using energy-filtered TEM (EFTEM) technique. The elemental distribution (mapping) obtained using this technique is shown in Fig. 4. Fig. 4(a) shows unfiltered TEM image. The corresponding zero-loss (elastic) and thickness map is shown in Fig. 4(b) and 4(c), respectively.Thickness map clearly showing that gains are having different thickness, so Z-contast image in Fig. 3(a) cannot tell exclusively different region of nanocomposite enriched by a particlular element having higher or lower Z-element. That is why we have carried out EFTEM imaging using core-loss region of different elements forming this nanocomposite structure. Chemical maps from La M (832 eV), and Pr M (931eV), Mn L (640 eV) and O K (532 eV) edges were obtained using jump-ratio method by acquiring two images (one post-edge and one pre-edge), respectively, to extract the background, with an energy slit of 20 eV. The composite image shown in Fig. 4(h) clearly indicates the presence of PCMO-LSMO nanocomposite structures.

The magnetic properties indicates the ferromagnetic nature of the nanostructure compounds. In Fig. 5 we have ploted the magnetization as function of external magnetic field at T = 5 K. Before starting the measurements samples were cooled down from T = 380 K in absence of any external magnetic field. Our measurement indicates the soft ferromagnetic nature of the compounds with very small corecivity (~ 50 Oe).

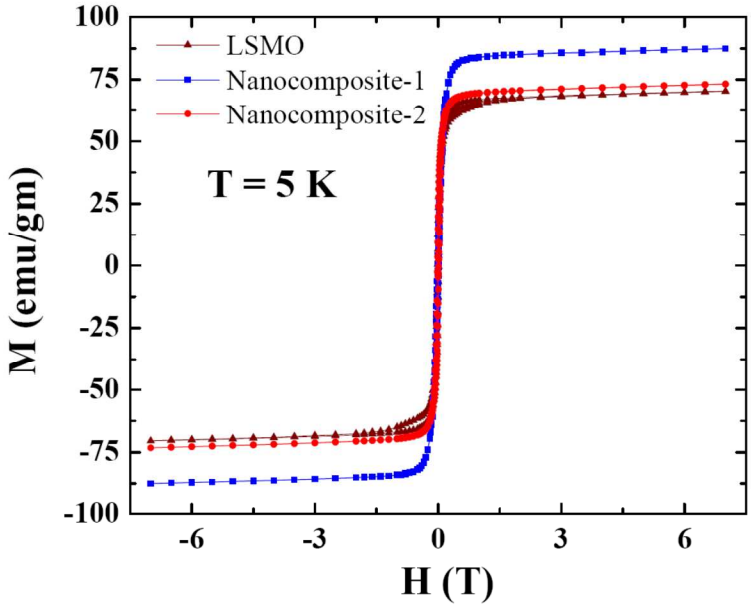

Figure 5. Magnetization as a function of external magnetic field for LSMO, nanocomposite-1 and nanocomposite-2 at T = 5 K.

Resistivity as a function of temperature in absence of external magnetic field shows metal insulator type transition near T = 210 K for the nanostructure compounds. The transition shifted towards the high temperature when external magnetic field was applied. At low temperature region (far below from metal insulator transition) compounds (LSMO, Nanocomposite-1 and Nanocomposite-2) shows an upturn in resistivity with lowering the temperature. This increasing nature of resistivity at low temperature is suppressed in the presence of external magnetic field. However the increasing nature persists even in presence of H = 8 T magnetic field.

RSC Advances Accepted Manuscript

To address the behavior of electrical resistivity at ferromagnetic metallic region several attempts have been made [27-30]. Jamie *el al*. proposed the origin about the generally observed dominant contribution of T^2 dependence term as due to the single magnon scattering [27]. However the interpretation by Zhao *et al.* raised the question about the validity of this model in case of manganites [28]. Taking in to account the electron- magnon scattering along with the electron-electron interaction Kubo *et al*. suggested the resistivity below metal insulator transition is given by [30]

$$\rho(T) = \rho_0 + \rho_2 T^2 + \rho_{4.5} T^{4.5} \quad \ldots\ldots\ldots\ldots\ldots\ldots\ldots\ldots (1)$$

In this model the resistivity due to temperature independent scattering process is represent by the term ρ_0 [30]. On the other hand $\rho_2 T^2$ indicate the electron-electron and $\rho_{4.5} T^{4.5}$ includes electron- magnon scattering [29]. The model represents our experimental data fairly well. We have fitted the experimental data from T = 200 K to T = 100 K by equation (1) and using the different coefficeints (ρ_0, ρ_2 and $\rho_{4.5}$) the data extrapolated below to T = 5 K. Fig. 6(a) shows the experimental resistivity data of the nanostructures and solid red line in this figure represents the fitting of resistivity data as a function of temperature by using the equation (1) in absence of external magnetic field. Similar good fitting also observed for temperature variation of resistivity data even in the presence of external magnetic field. In this context it should be mentioned that at the low temperature region especially below T = 80 K the deviation between the experimental and calculated resistivity data was observed. Quantitavely the deviation [$\delta\rho$ = ρ(expt.) – ρ(calculated)] is ploted in inset of the Fig. 6(a). It is well documented that at high temperature region especially above the metal insulator transition the electronic transport is governed through the small polaron hopping. Mathematical representation of resistivity as a function of temperature is given by

$$\rho(T) = AT exp\left(\frac{E_a}{K_B T}\right) \quad \ldots\ldots\ldots\ldots\ldots\ldots\ldots\ldots (2)$$

RSC Advances Accepted Manuscript

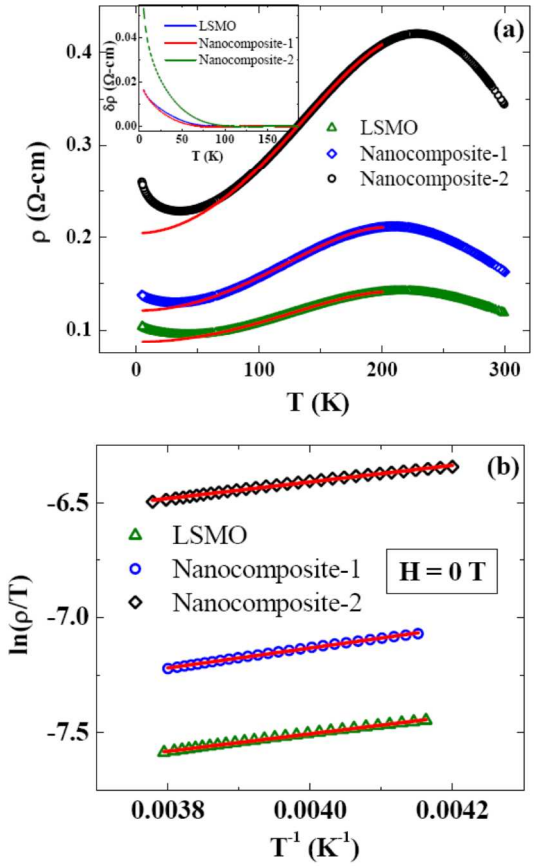

Figure 6. (a) Resistivity as a function of temperature in metallic region for LSMO, Nanocomposite-1 and Nanocomposite-2 nanostructure in absence of magnetic field. Solid red line represents the fitting curve of experimental data by using equation (1). Inset of (a) represents the deviation between experimental and calculated resistivity . (b) Fit to the resistivity data of nanostructures according to the adiabatic small polaron hopping above metal insulator transition in absence of external magnetic field.

Where 'A' is temperature independent coefficient, E_a is activation energy of polaron and K_B is Boltzmann constant.

The fitting of the experimental data for LSMO and Nanocomposites for insulating region by using equation (2) is given in Fig. 6(b). Activation energy E_a has been calculated from the slope of the fitted line and it was found to be ~ 32.6 meV, ~ 37.38 meV and ~ 36.55 meV for LSMO, nanocomposite-1 and nanocomposite-2 respectively. Another fitting parameter 'A' can be calculated by extrapolation of liner fitted line shown in Fig. 6(b). Calculated value of 'A' is 1.21×10^{-4} Ω-cm/K, 1.40×10^{-4} Ω-cm/K and 3.04×10^{-4} Ω-cm/K for LSMO, nanocomposite-1 and nanocomposite-2 respectively. According to the Worledge *et al.* the coefficient 'A' is connected with number density of charge carrier [32]. The observation of low temperature minima in resistivity is almost a generic behavior of ferromagnetic granular materials [19-22]. Numerous models have been proposed to explain this phenomenon. In case of polycrystalline manganites it is attributed to Coulomb Blockade (CB) [33] or electron-electron interaction [33]. Considering bulk scattering model including quantum correction to conductivity, Rozenberg *et al.* argued that this model strongly disagrees with the experimental data for ceramic manganites as the resistivity minima is present

RSC Advances Accepted Manuscript

even in finite magnetic field [21]. On the other hand for strongly field dependent minima of resistivity at low temperature for granular materials intergranular spin polarized tunneling model (SPT) is proposed [35]. According to this model the depth of the resistivity minima decreases with increase of magnetic field and at a particular field value it vanishes. The simplified functional form of resistivity at low temperature considering tunneling through the grain boundary is given by [36]

$$\rho(T,H) = \frac{r_1 + r_2 T^{\frac{3}{2}}}{1 + \epsilon < cos\theta_{ij} >} \ldots\ldots\ldots\ldots\ldots\ldots\ldots (3)$$

Where r_1 and r_2 are field independent parameter and ϵ is related with the degree of polarization of the charge carriers in each granule. In absence of external magnetic field the spin correlation function $< cos\theta_{ij} >$ is represented by

$$< cos\theta_{ij} >= -L\left(\frac{|J|}{K_B T}\right) \ldots\ldots\ldots\ldots\ldots\ldots\ldots\ldots\ldots\ldots\ldots (4)$$

Here L(x) = [coth(x) – 1/x] is the Langevin function and 'J'is the inter grain antiferromagnetic exchange integral. In presence of external magnetic field Ciftja *et al.* deduce the analytical expression for spin correlation function which is given by [37]

$$< cos\theta_{ij} >= \frac{1}{4} + \frac{1}{3 + exp\left(\frac{-3J_S}{K_B T}\right)} \ldots\ldots\ldots\ldots\ldots\ldots\ldots\ldots (5)$$

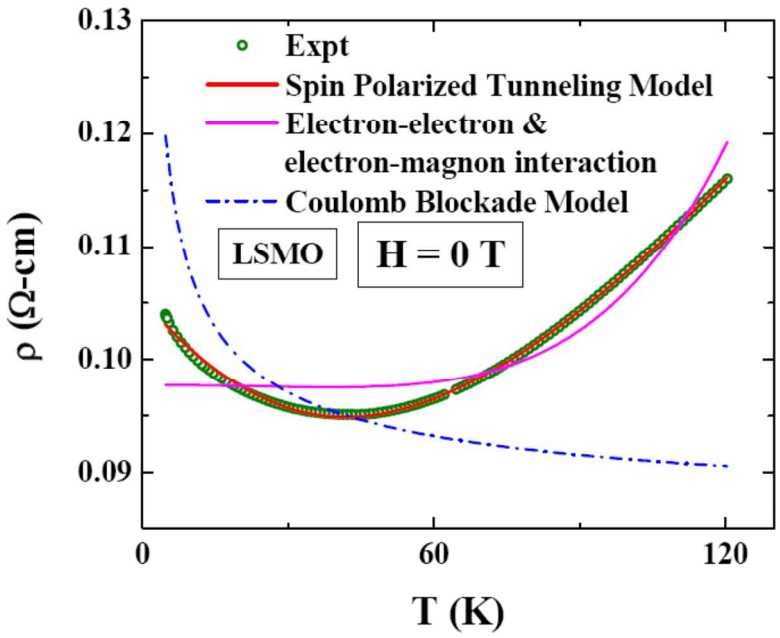

Figure 7. Temperature dependent resistivity in the absence of external magnetic field at low temperature region of LSMO nanoparticles are fitted by using several models.

RSC Advances Accepted Manuscript

Here J = S(S+1)J_S, S is the atomic ion spins [35]. Similar upturn trend of resistivity is also expected for CB effect in granular system. Sheng *et al*. deduce the expression describing the increasing nature of resistivity at low temperature which is given by

$$\rho(T) = A\, exp\left(\sqrt{(\Delta/T)}\right) \dots\dots\dots\dots\dots\dots\dots\dots\dots\dots (6)$$

where 'A' is fitting parameter and $\Delta \sim E_C$ is energy barrier [38]. The presence of CB contribution in resistivity of manganites has been studied by several authors. As for example Balcells *et al*. made the experimental estimation of the CB effect in resistivity for $La_{0.7}Sr_{0.3}MnO_3$ having different grain sizes [14]. In addition to that Dey *et al*. showed that for single phase nanocrystalline $La_{0.7}Ca_{0.3}MnO_3$ of particle size 14-27 nm, the low temperature upturn in resistivity can be well described considering CB effect [39]. In this present manuscript we also check the fitting of experimental data by using different model for both the compounds. As a representative picture we have shown the fitting of experimental ρ(T) data only for LSMO at H = 0 T using three different model namely CB model, combining electron-electron and electron-magnon interaction and SPT model. Our analysis suggests that except SPT model good agreement with experimental data is not found for other models (Fig. 7). Generally CB effect is observed for very small grain size. The disagreement of CB model and experimental data in our present study is possible due to the larger grain size of the compounds. Similarly disagreement of the experimental data with the combined electron-electron and electron-magnon interaction indicates that these were weaker in the present case.

In our present case upturn in resistivity at low temperature region for all compounds are suppressed but not completely vanishes even in 8 T external magnetic field. Therefore we treat the problem in the light of inter grain tunneling model. Temperature variation of resistivity at low temperature for LSMO and nanocomposite compounds in absence of magnetic field are fitted by using equations (3) and (4) whereas equations (3) and (5) are used to fit the experimental data taken in the presence of external magnetic field. In both cases the excellent fit was observed and which displayed in Fig. 8.

RSC Advances Accepted Manuscript

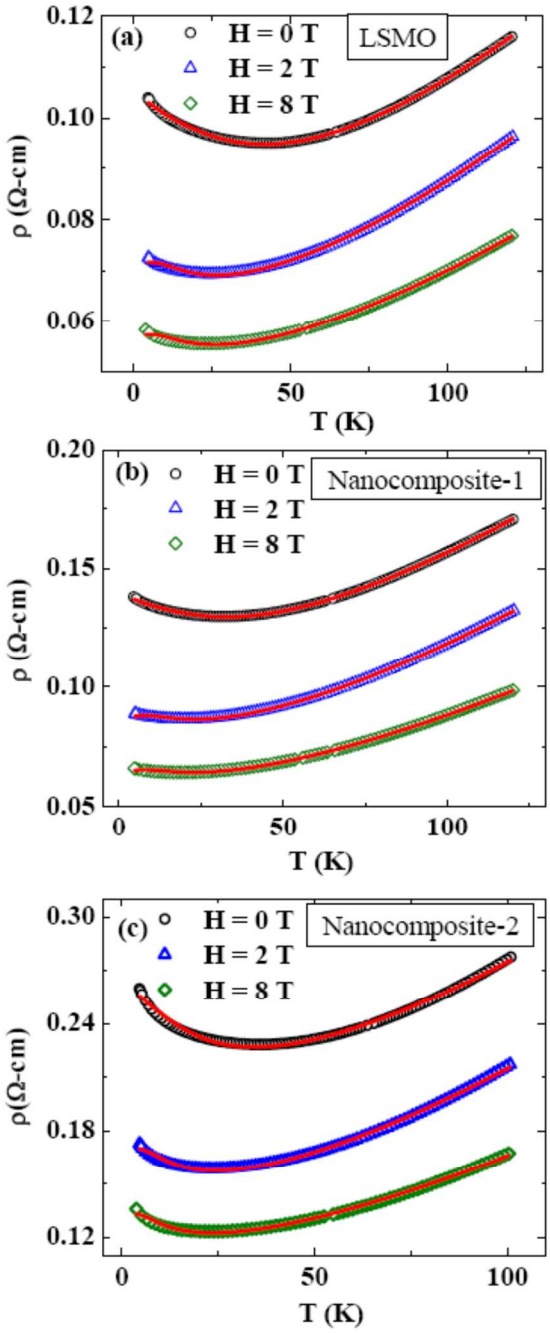

Figure 8. (a), (b) and (c) Electrical resistivity of LSMO nanoparticles, Nanocomposite-1 and Nanocomposite-2 at low temperature region in absence and in presence of external magnetic field. Solid line (red line) is represent the fitting curve by using equation (3)

External magnetic field dependence of magnetoresistance (MR) [MR = {R(H)-R(0)}/R(0)] at different temperature of LSMO and Nanocomposites is displayed in Fig. 9.

RSC Advances Accepted Manuscript

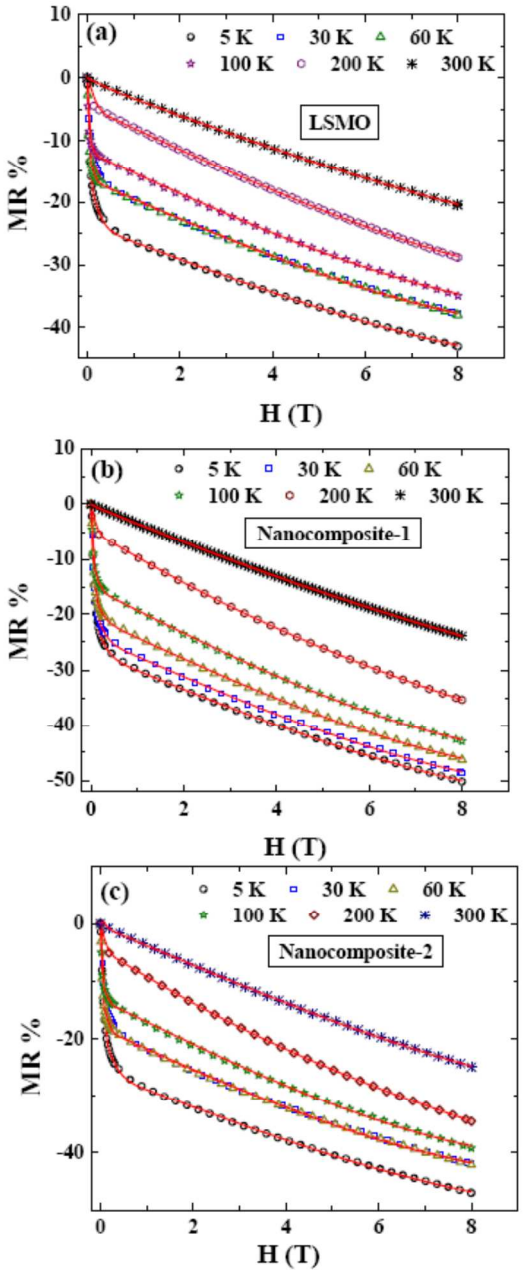

Figure 9. Magnetoresistance (MR) as a function of magnetic field for (a) LSMO and (b) Nanocomposites. Solid red line represents the fitted data using equation (7).

Sharp increasing nature of the magnitude of MR at low magnetic field was observed in both cases which is analogous to the typical ferromagnetic granular materials at low temperature. This sharp drop of MR can be explained by taking into account intergranular spin polarized tunneling. According to Hwang *et al.* movement of magnetic domain walls through the grain boundaries due to the application of external magnetic field is associated

RSC Advances Accepted Manuscript

with the progressive alignment of magnetic domains, as a result the sharp drop of MR at low field was observed [18]. In addition to that, MR slightly increases in case of nanocomposites compared to LSMO. From the magneto-transport measurements (resistance as a function of external magnetic field, R(H)), we have calculated MR by using the above mentioned expression. The numerical value of the resistance at T = 30 K and 60 K (at low field region) are very close to each others for LSMO and nanocomposite-2 compound. Whereas R(H) at T =30 K and 60 K shows almost parallel nature at the high magnetic field region. As a result the quantitative value of MR (at T= 30 K and 60 K) were overlapped maintaing a small difference at low field region for the nanostructures LSMO and nanocomposite-2.

To explore the main role behind this enhancement of MR in nanocomposite type nanostructures our primary objective is to separate out the different contributions of MR, originating from SPT (MR_{SPT}) and from suppression of spin fluctuation owing to the applied magnetic field (MR_{INT}). Considering the response of gradual slippage of domain walls across the grain boundaries pinning centers Raychaudhuri *et al*. proposed a phenomenological model for MR based on SPT [40]. According to this model expression of MR is

$$MR = -\tilde{A}\int_0^H f(K)dK - JH - KH^3 \quad \text{..... (7)}$$

Here J, H and K are field independent constants. While f(K) is defined by the pinning strength of the grain boundaries pinning centers and it is consisted as the weighted average of a Gaussian and skewed Gaussian distribution which is given by

$$f(K) = Aexp(-BK^2) + CK^2exp(-DK^2) \quad \text{..... (8)}$$

By using the value of the fitting parameters A, B, C, D, J and K (since Ã is absorbed in A and C) one can separate out MR_{SPT} and MR_{INT} parts from total MR by following way

$$MR_{SPT} = -\int_0^H f(K)dK \quad \text{..... (9)}$$

$$MR_{INT} = -JH - KH^3 \quad \text{..... (10)}$$

To fit the MR data of the nanostructure compounds, we have followed the same procedure as considered by Raychaudhuri *et al.* [40]. According to their model the derivative of the MR as a function of the external magnetic field is given by

$$\frac{d(MR)}{dH} = Aexp(-BH^2) + CH^2exp(-DH^2) - J - 3KH^2 \quad \text{..... (11)}$$

By differentiating our experimental MR data with respect to H, we have fitted the d(MR)/dH as a function of H curve using the equation (11) and extracted the best fitting parameters for different temperatures. Using those best fitting parameters we have calculated MR as afunction of H from the equation (7). The variation of MR with external magnetic field along with the fitted line for LSMO and Nanocomposites are shown in Fig. 8.

By using the best fitted parameters at different temperature we have calculated temperature dependence of MR_{SPT} and MR_{INT} for both compounds from the equation (9) and (10) respectively. The variation of the MR_{SPT} and MR_{INT} is ploted in Fig. 10(a) and 10(b) respectively.

RSC Advances Accepted Manuscript

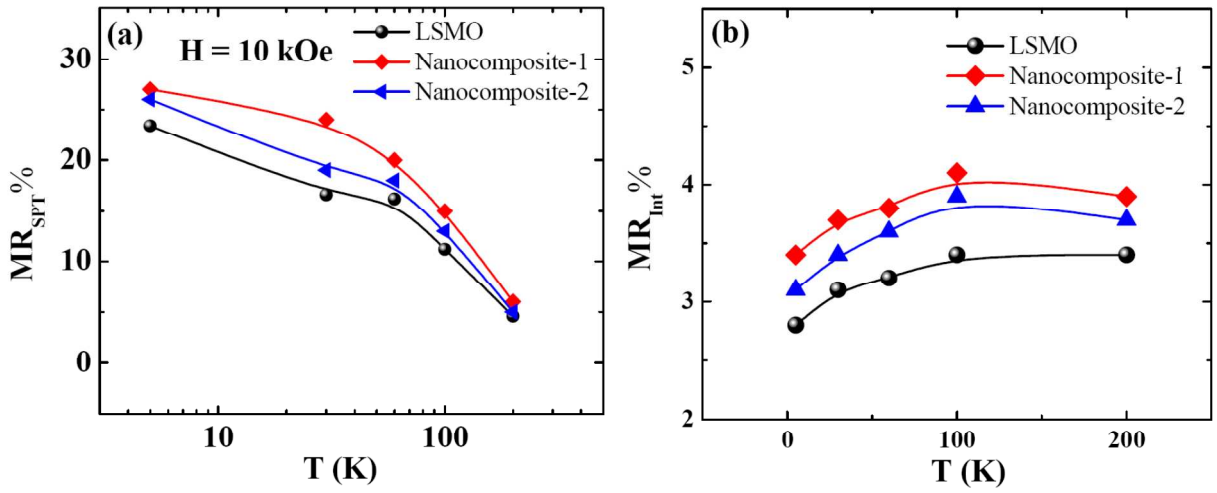

Figure 10. (a) Temperature dependence of MR_{SPT} for LSMO and Nanocomposites at H = 10 kOe magnetic field. (b) Temperature variation of MR_{INT} for those compounds at same magnetic field H = 10 kOe.

From Fig. 10(a) it is clear that MR_{SPT} is enhanced in nanocomposites compared to LSMO nanoparticles. This interesting behavior of nanocomposites can be explained considering the effect of extra grain boundaries of PCMO in LSMO matrix compared to LSMO nanoparticles. It is also reported that MR_{SPT} is very sensitive with the behavior of the grain boundaries. Dey *et al*. studied the magneto-transport properties of $La_{0.7}Ca_{0.3}MnO_3$ nanoparticles (down to 17 nm). They observed that MR_{SPT} increases and it is almost constant with decreasing particle size (*i.e.* enhanced grain boundaries effect) across a wider temperature range [39]. External magnetic field, we examined the low and high field magnetoconductivity data of our two compounds. To elucidate this we have adopted the model proposed by Lee *et al*. [25]. According to their model magnetoconductivity (σ) as a function of magnetic field is given by the simplified relation

$$\frac{\sigma}{\sigma_0} = \left(\frac{\sigma}{\sigma_0}\right)_{LF} + S(T)H \ldots\ldots\ldots\ldots\ldots\ldots\ldots\ldots\ldots\ldots\ldots\ldots (12)$$

Where $\left(\frac{\sigma}{\sigma_0}\right)_{LF}$ terms corresponds the low field magnetoconductance which depends on the different magnetization orientation of neighboring grains. Whereas the term S(T)H is connected with the magnetic behavior of the grain boundaries.

RSC Advances Accepted Manuscript

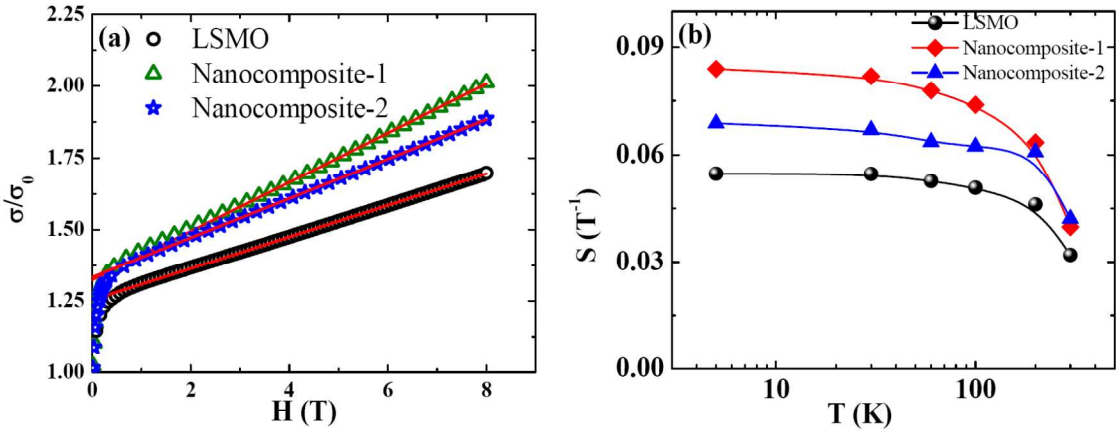

Figure 11. (a) The magnetic field variation of magnetoconductivity at T = 5 K for LSMO and Nanocomposites along with liner fitting at high field region. (b) Grain boundaries spin susceptibilities as a function of temperature for LSMO and Nanocomposites.

By fitting our experimental magnetoconductivity as a function of magnetic field data at the high field region using equation (12) we have extracted the surface spin susceptibility 'S' at different temperatures. One typical linear fitting of magnetoconductance as a function of magnetic field for LSMO and Nanocomposite at T = 5 K is shown in Fig. 11(a). It is worth noting that observed low field magnetoconductance of nanocomposite is very close to universal limit through second order tunneling [25]. The temperature dependence of surface spin susceptibility 'S' of LSMO and Nanocomposites are presented in Fig. 11(b). Very interestingly we found that the nature of the S(T) is qualitatively similar as the $MR_{SPT}(T)$. Quantitatively we also found that surface spin susceptibility increases in our nanocomposites similar as MR_{SPT}. From this comparative analysis of our transport and magnetotransport data it indicates that the behavior of MR is decided predominantly by the nature of the response of surface magnetization of those nanosized magnetic particles, as suggested by Lee *et al.* [25].

From the magnetic and magneto-transport measurements we observe that the charge ordered-ferromagnetic nanocomposites shows the qualitatively same behavior as LSMO. However due to the effect of the artificial grain boundaries in nanocomposite nanostructures the responses are differ quantitatively with respect to its parent ferromagnetic LSMO nanoparticles. It is worthmentioning that the properties of the nanocomposite compounds also quantitatively modifies depending upon their sintering temperatures which is mentioned in the sample preparation part.

RSC Advances Accepted Manuscript

4. Concluding Remarks

To summarize, we have synthesized PCMO-LSMO nanocomposites as well as LSMO nanoparticles by sol-gel route. The effect of the artificial grain boundaries on transport and magnetotransport properties of the prepared charge ordered-ferromagnetic nanocomposites have been investigated. Low temperature upturn in resistivity for all the compounds are well described by spin polarized tunneling model. Enhanced magnetoresistance and low field magnetoconductance in case of the nanocomposites compared to the LSMO nanoparticles are analyzed considering the second order tunneling mechanism through the grain boundaries. Our study indicates that the spin polarized tunneling in these kind of compounds play the dominant role for the rise in resistivity with lowering temperature in low temperature region and also for the low field magnetoresistance.

Acknowledgements

One of the author Kalipada Das would like to sincerely acknowledge CSIR-INDIA for the fellowship. We thank Pallab Bag and R. Rawat, UGC-DAE Cosortium for Scientific Research, Indore for magnetoresistance measurements and Sudipta Mondal, SINP, Kolkata, for help in x-ray data analysis.

References

[1] Y. Tokura, *Colossal Magnetoresistive Oxides*, (Gordon and Breach Science, Amsterdam, 2000).

[2] H. Kuwahara, Y. Tomioka, A. Asamitsu, Y. Moriotomo and Y. Tokura, *Science,* 1995, **270**, 961.

[3] A. Biswas, I. Das and C. Majumdar, *J. Appl. Phys*., 2005, 98, 124310.

[4] A. Biswas and I. Das, *Phys. Rev. B.*, 2006, 74, 172405.

[5] A. Biswas, T. Samanta, S. Banerjee and I. Das, *Appl. Phys. Lett.,* 2009, 94, 233109.

[6] J. Ding, Z. Lin, J. Wu, Z. Dong and T. Wu, Anisotropic Imprint of Amorphization and Phase Separation in Manganite Thin Films via Laser Interference Irradiation. Small. doi: 10.1002/smll.201400555 (2014).

[7] A. Biswas and I. Das, *Appl. Phys. Lett*., 2008, 92, 012502.

RSC Advances Accepted Manuscript

[8] M. Uehara, S. Mori, C. H. Chen and S. W. Cheong, *Nature (London)*, 1999, 399, 560.

[9] L. Zhang, C. Israel, A. Biswas, R. L. Greene and A. de Lozanne, *Science,* 2002, 298, 805.

[10] S. Dong, R. Yu, S. Yunoki, J. M. Liu and E. Dagotto, *Phys. Rev. B.,* 2008, 78, 064414.

[11] H. Y. Hwang, S. W. Cheong, P. G. Radaelli, M. Marezio and B. Batlogg, *Phys. Rev. Lett.*, 1995, 75 , 914.

[12] P. Lyu and D. Y. Xing, *Phys. Rev. B.,* 1998, 58 , 54.

[13] M. Viret, M. Drouet, J. Nassar, J. P. Contour, C. Fermon and A. Fert, *Europhys. Lett.,* 1997, 39, 545.

[14] L . I. Balcells, J. Fontcuberta, B. Martnez and X. Obradors, *Phys. Rev. B.*, 1998, 58 , R14697.

[15] R. Shreekala, M. Rajeswari, K. Ghosh, A. Goyal, J. Y. Gu, C. Kwon, Z. Trajanovic, T. Boettcher, R. L. Greene, R. Ramesh and T. Venkatesan, *Appl. Phys. Lett.*, 1997, 71 , 282.

[16] A. de Andres, M. Garca-Hernandez and J. L. Martnez, Phys. Rev. B., 1999, 60 , 7328.

[17] P. Wagner, I. Gordon, L. Trappeniers, J. Vanacken, F. Herlach, V. V. Moshchalkov and Y. Bruynseraede, *Phys. Rev. Lett.,* 1998, 81, 3980.

[18] H. Y. Hwang, S. W. Cheong, N. P. Ong and B. Batlogg, *Phys. Rev. Lett*., 1996, 77, 2041.

[19] S. Das and T. K. Dey, *Solid State Commun.,* 2005, 134 , 837.

[20] S. Das and T. K. Dey, *Journal of Magnetism and Magnetic Materials.,* 2005, 294, 338.

[21] E. Rozenberg, M. Auslender, I. Felner, and G. Gorodetsky, *J. App. Phys.,* 2000, 88, 2578.

[22] S. Mukhopadhyay, I. Das, *Euro Phys. Lett.,* 2007, 79, 67002.

[23] L. Balcells, L. Abad, H. Rojas, A. P. del Pino, S. Estrade, J. Arbiol, F. Peiro and B. Martinez, *small*, 2008, 4, 365.

[24] Y. Wang and H. J. Fan, *small*, 2012, 8, 1060.

RSC Advances Accepted Manuscript

[25] S. Lee, H. Y. Hwang, B. I. Shraiman, W. D. Ratcliff and S. W. Cheong, *Phys. Rev. Lett.,* 1999, 82, 4508.

[26] P. G. Radaelli *et al.*, *Phys. Rev. B.,* 1997, 56, 8265

[27] M. Jaime, P. Lin, M. B. Salamon and P. D. Han, *Phys. Rev. B.,* 1998, 58, R5901

[28] G. Zhao, V. Smolyaninova, W. Prellier and H. Keller, *Phys. Rev. Lett*., 2000, 84, 6086.

[29] G. Jeffrey Snyder, R. Hikes, S. DiCarolis, M. R. Beasley and T. H. Geballe, *Phys. Rev. B.*, 1996, 53, 14434.

[30] K. Kubo and N. A. Ohata, *J. Phys. Soc. Jpn.,* 1972, 33, 21.

[31] A. S. Alexandrov and A. M. Bratkovsky, *Phys. Rev. Lett.*, 1999, 82, 141.

[32] D. C. Worledge, G. Jeffrey Snyder, M. R. Beasley, T. H. Geballe, R. Hiskes and S. DiCarolis, *J. Appl. Phys.*, 1996, 80, 5158.

[33] M. Garcia-Hermandez, F. Guinea, A. de Andres, J. L. Martinez, C. Prieto and L. Vazquez, *Phys. Rev. B.,* 2000, 61, 9549.

[34] A. Tiwari and K. P. Rajeev, *Solid State Commun.*, 1999, 111, 33.

[35] J. S. Helman and B. Abeles, *Phys. Rev. Lett.*, 1976, 37, 1429 .

[36] M. I. Auslender, E. Rozenberg, A. E. Karlin, B . K. Chaudhuri and G. Gorodetsky, *J. Alloys Compounds.*, 2001, 326, 81.

[37] O. Ciftja, M. Luban, M. Auslender and J. H. Luscombe, *Phys. Rev. B.,* 1999, 60, 10122.

[38] P. Sheng, B. Abeles and Y. Arie, *Phys. Rev. Lett.*, 1973, 31, 44.

[39] P. Dey and T. K. Nath, *Phys. Rev. B.,* 2006, 73, 214425.

[40] P. Raychaudhuri, K. Sheshadri, P. Taneja, S. Bandyopadhyay, P. Ayyub, A. K. Nigam and R. Pinto, *Phys. Rev. B.*, 1999, 59, 13919.

RSC Advances Accepted Manuscript